



Simplified displacement-based economic loss assessment of single-story steel buildings: simplified vs. full 3D models

Gaetano Cantisani^a, Gaetano Della Corte^a

^a *Dipartimento di Strutture per l'Ingegneria e l'Architettura, Università di Napoli Federico II, Napoli, Italy*

Keywords: Earthquake, damage, loss, model, steel

ABSTRACT

With reference to old non-residential single-story steel buildings, the paper presents comparisons of different models for economic loss assessment using a simplified displacement-based procedure. Starting from non-linear static analysis, the simplified displacement-based loss assessment method is a limit-states approximation of the real (continuous) economic loss process. Different finite element (FE) models were considered: (i) a finite element model of the entire 3D structure, including envelope panel response; (ii) two alternative simplified representations of the seismic response using finite element models of 2D frames extracted from the 3D structure. The FE models were built within the OpenSEES software platform. Comparisons of results from the different structural models are illustrated, in terms of loss curves (i.e., monetary losses vs. mean annual frequency of exceedance of the earthquake intensity) and expected (economic) annual losses (EAL). Based on such comparisons, conclusions are drawn about advantages and disadvantages of using the various structural models for the loss assessment.

1 INTRODUCTION

Structural analysis generally provides technical information concerning the whole response of buildings due to seismic actions. However, commuting technical information into variables clearly understood by building owners is an important consideration to allow for conscious and responsible decision making. From this perspective, economic loss assessment is a powerful tool. As the economic loss assessment is one step forward the structural analysis itself, there is more than one way to perform it. The traditional approach is related to the performance-based earthquake engineering guidelines and procedures [Porter, 2003]. The framework is detailed in FEMA P-58-1 [2012] via a four-stage process of (i) hazard analysis, (ii) structural analysis, (iii) damage analysis and (iv) loss analysis. In this approach, the structural analysis step is generally carried out using non-linear dynamic analysis via several ground motions input to consider record-to-record variability. This choice clearly leads to several issues: (i) the necessity to have adequate knowledge for modelling non-linear behaviour in cyclic loading conditions at both material and component levels;

(ii) a large amount of computational time necessary to perform the analysis, as well as availability of powerful computers. As a simplification, methods utilizing direct displacement-based design concepts have been proposed [Welch et al., 2014]. Using results arising from pushover analysis, the loss assessment process can be readapted. As a result, a direct displacement-based loss assessment (DBLA) procedure is obtained. Nevertheless, in engineering practice it is still difficult to build non-linear 3D finite element (FE) models to simulate the whole building response with realistic component damages. Therefore, the aim of this paper is to compare the DBLA results for FE models of varying degrees of complexity. To this aim, an archetype non-residential single-story steel building was adopted as case study. The paper shows comparisons in terms of loss analysis applied to: (i) a full 3D model with a relatively complex representation of the building envelope and connection responses, (ii) a simplified 3D model obtained from the assemblage of the response of 2D frames, considering a few key aspects in the modelling of the non-linear response and using some engineering judgment to consider interaction phenomena between the bare structure and the

envelope response. After discussing about the archetype geometry and other important assumptions, the paper focuses on a description of the FE models and the inventory of the damageable components used to perform the economic loss analysis. Then, the paper shows comparisons of results, tracing conclusions concerning the assumptions made and their effects on the analysis results.

2 CASE STUDY STRUCTURE

The case study building structure was an old non-residential single-story steel building. Figure 1 shows frontal and plan views of the building, providing also essential information about the cladding and roofing.

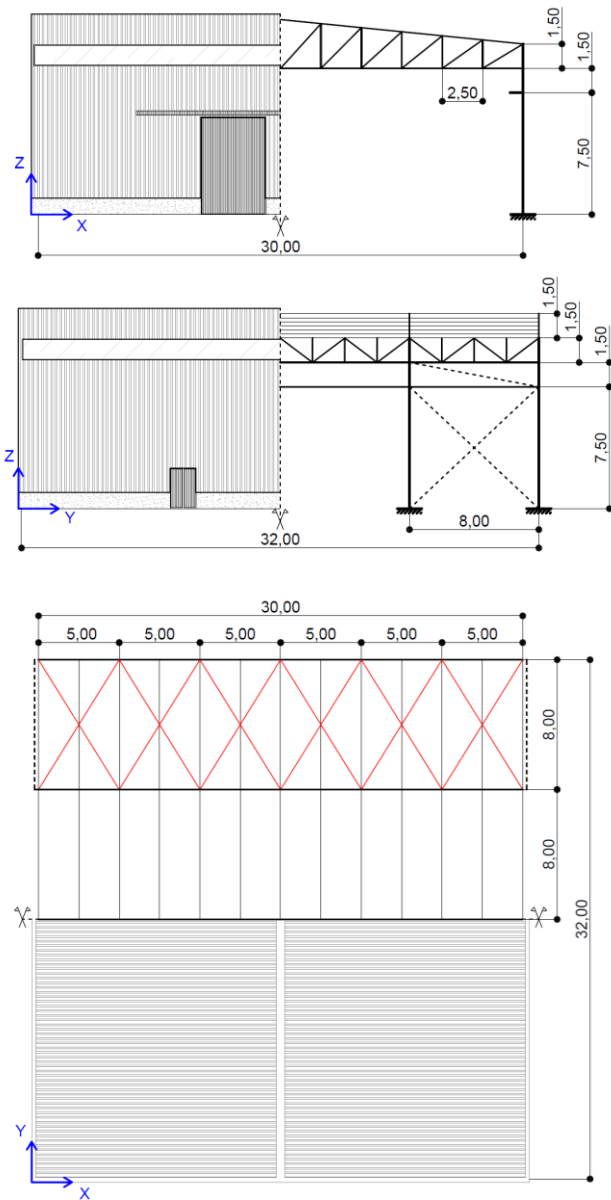


Figure 1. Case study global geometry.

The building was made of five main trusses in the transverse direction (X), and concentrically braced frames in the longitudinal direction (Y). The building structure was designed following the code and standards of practice used in the decade 1980s-1990s in Italy [CS.LL.PP. 1982, CS.LL.PP. 1986, CNR-UNI 10011]. Accordingly, the design was simulated using the allowable stress method, assuming “Fe 430” steel grade (allowable stress = 190 MPa). Two load combinations were considered for the design (main vertical and lateral load combinations), but neither capacity design rules nor ductility detailing were considered. Figure 2 summarizes the output of the simulated design in terms of member cross sections. The design of the portal frames in the X-direction was governed by the gravity load combination for both members and connections. Instead, the design of the braced frames in the Y-direction was governed by brace slenderness limitations ($\lambda \leq 200$). The column section was selected to satisfy a roof drift limitation of $1/500 H$ ($H = 10.50 \text{ m}$).

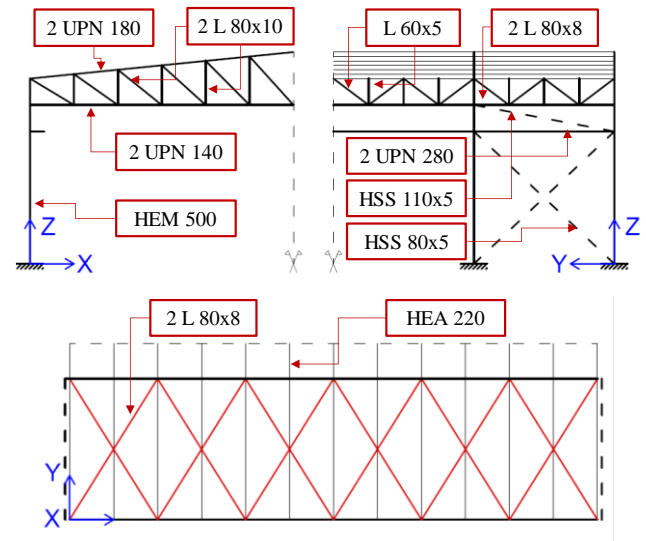


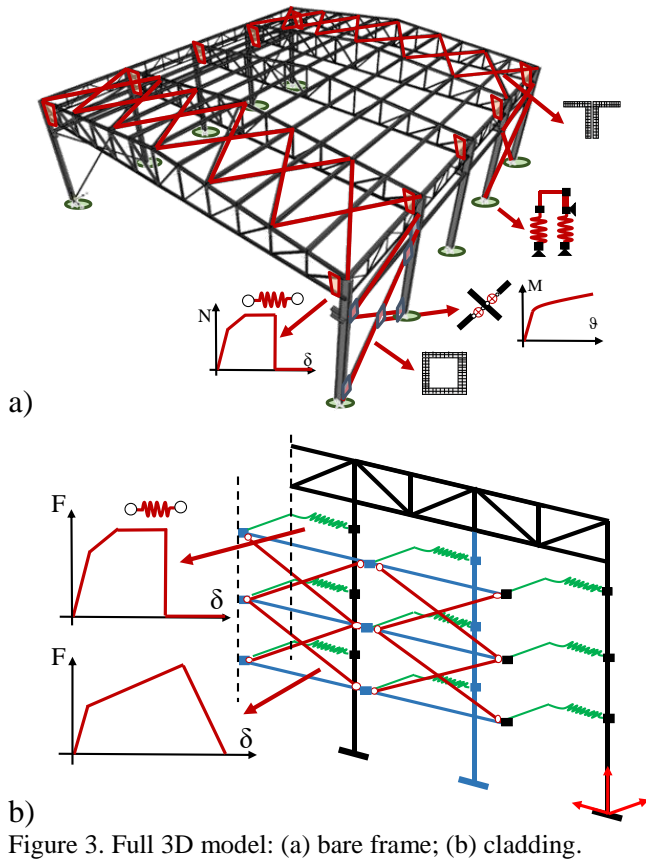
Figure 2. Case study member cross sections.

3 MODELLING ISSUES

3.1 3D model

A 3D model was built within OpenSEES [McKenna *et al.*, 2010]. Figure 3(a) summarizes the main features of the bare frame model: (i) braces were modelled with initial imperfections, non-linear fiber discretization of cross sections, and additional non-linear springs to simulate out-of-plane bending of gusset plates; (ii) column base anchors were modelled by non-linear fiber elements to simulate the axial-shear force-

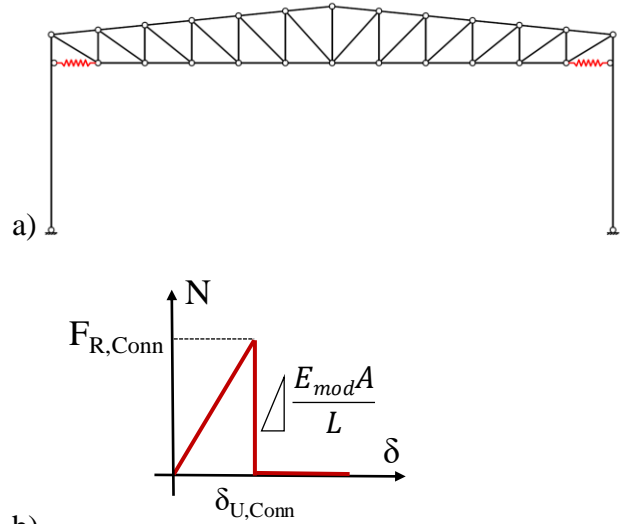
deformation interaction; (iii) truss-to-column connections were modelled using springs with a tri-linear force-deformation response to simulate shear failure of bolts. Figure 3(b) shows a sketch representing the envelope model in a longitudinal view. A couple of equivalent diagonal truss elements were used to consider each cladding and roofing panel module. Two types of cladding were considered: (i) sandwich panels (SP); (ii) (single-skin) trapezoidal sheeting (TS). In addition, cladding panel to secondary steelwork connections were explicitly represented in the model using force-deformation characteristics similar to those adopted for truss-to-column connections. The same modelling approach was adopted to include roofing panels. Detailed information concerning the 3D model can be found in Cantisani and Della Corte [2018].



3.2 Simplified 3D model

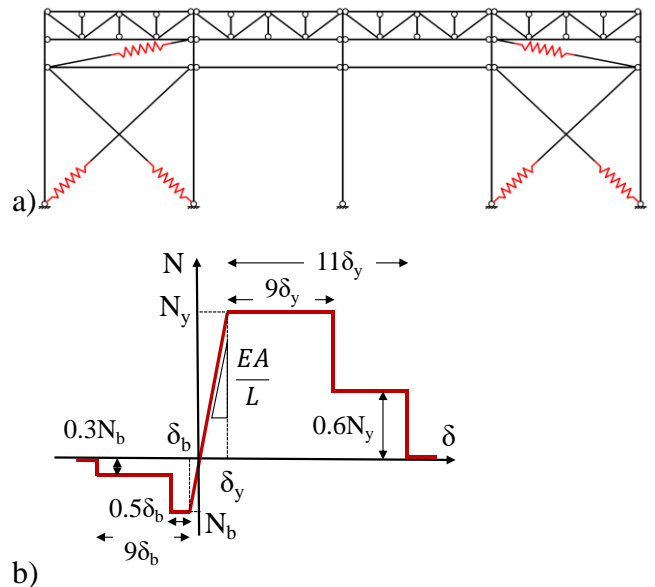
A simplified 3D model was built by extracting 2D frames from the 3D building structure. Figure 4(a) shows a sketch of the 2D frame model in the transverse direction, with indication of the non-linear springs used to characterize the inelastic behaviour of the portal frame. In addition, Figure 4(b) shows the implemented model for the truss-to-column connections, which was built starting from application of Eurocode 3 [CEN EN 1993-

1-1] for both stiffness (E_{mod}) and resistance ($F_{R,conn}$) calculations. Brittle behaviour was assumed when the force demand exceeded the connection force capacity.



b) Figure 4. 2D frame model for the transverse direction: (a) model sketch; (b) truss-to-column connection response.

Figure 5(a) shows a sketch of the 2D frame model in the longitudinal direction. Nonlinear truss elements were adopted to represent the brace response. Figure 5(b) shows the adopted force-displacement response for the brace-equivalent truss element [ASCE SEI 41-13].



b) Figure 5. 2D frame model for the longitudinal direction: (a) model sketch; (b) brace response.

In the 2D model, the cladding model was also simplified. First, a uniform distribution of drifts along the height of the structure in a given cladding plane was assumed. Then, starting from consideration of a single panel sub-assembly [Cantisani and Della Corte, 2018], series and parallel springs were composed to represent the

entire panel assembly. As in the case of the 3D model, both sandwich panels (SP) and trapezoidal sheeting (TS) were alternatively considered. Figure 6(a) and Figure 6(b) show the cladding response in terms of shear force (V_{CL}) vs. drift ratio (d/H , $H=10.50\text{ m}$) response, respectively for the transverse and longitudinal directions. In the simplified model, a rigid diaphragm behaviour was assumed at the roof, with no limits to the resistance (i.e., both the roofing panels and roof braces deformations were neglected). The overall building response was obtained by summing the individual responses of the 2D frames and the cladding for the two main building directions.

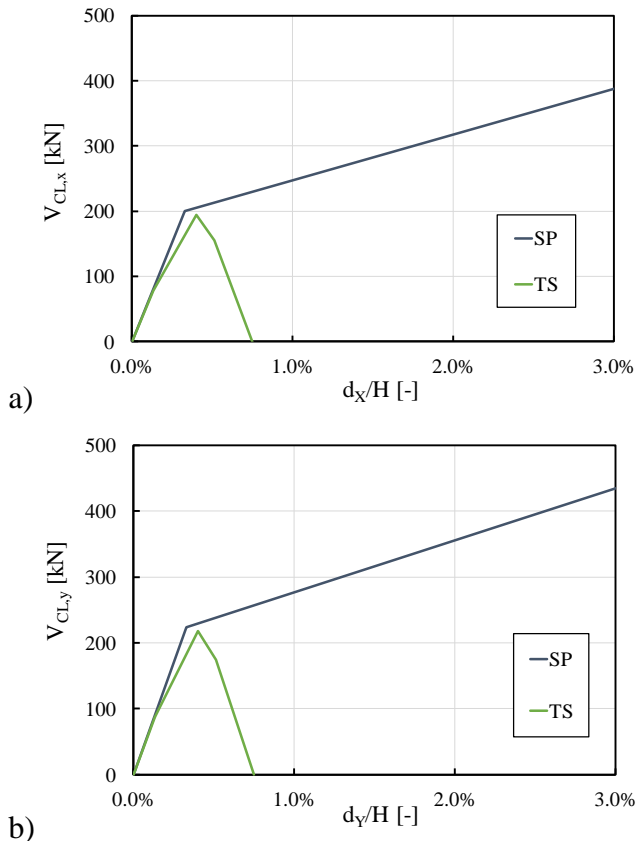


Figure 6. Simplified cladding model: (a) transverse (X-) direction; (b) longitudinal (Y-) direction.

4 INVENTORY OF DAMAGEABLE COMPONENTS

To perform a loss assessment, damageable components must be identified, in terms of damage states and consequence functions (i.e. repair cost and repair time for each damage state). The following sections provide a summarized description of the inventory and modelling of damageable components for the case study building. It is important to emphasize that consideration of non-structural components, such as electrical and plumbing systems or the

building content, was out of the scope of this work, which is instead focused on the relative importance of various steel structure modelling assumptions.

4.1 Damage modelling

The damageable components from the bare structure were identified using the pushover analysis results: truss-to-column connections, column base connections, roof braces, vertical braces, and foundation anchors. In addition, both cladding and roofing panels were included in the inventory of damageable components for the 3D model. For each component, an appropriate engineering demand parameter (EDP) was selected to evaluate the damage. On the contrary, in the case of the simplified models damage of roofing panels and roof braces components was neglected. Indeed, rigid diaphragm behaviour was assumed for the roof.

4.2 Component fragilities

For each damageable component and damage state (DS), fragility functions were built assuming a lognormal distribution. Information concerning several components and relevant damage states were obtained using the database available within the software PACT [FEMA P-58-1]. Where fragilities were not available from the literature, median and dispersion of the associated lognormal distributions were estimated using some engineering judgement. As an example, Figure 7(a) shows the fragility functions built for the sandwich panels (SP), starting from a discretization of the backbone curve into four damage states (DSs). Figure 7(b) shows the associated repair costs for each DS.

5 DBLA METHODOLOGY DESCRIPTION

This section summarizes the procedure adopted to evaluate expected economic losses (Figure 8). Starting from the pushover curve of the actual structure, an equivalent single degree of freedom (SDoF) system was first defined. On the pushover curve, significant limit states were identified as a discretization of the continuous structural response. Then, each limit state was identified as a point of the equivalent SDoF pushover curve. Each point was characterized by an effective displacement ($\Delta_{eff,i}$) and an effective base shear force ($V_{B,i}$). Given the point, the associated (secant) stiffness ($k_{eff,i}$) and,

consequently, the associated effective period of vibration ($T_{eff,i}$) were evaluated. Then, the vector $[\Delta_{eff,i}, T_{eff,i}]$ was plotted together with equivalent highly-damped displacement response spectra ($\xi_{eq,i}$ = equivalent viscous damping). Interpolating values of displacement spectra for a given value of the effective period, the return period (T_R) associated to the elastic displacement response spectrum passing through the point $[\Delta_{eff,i}, T_{eff,i}]$ was calculated. Then, the earthquake return periods ($T_R(\Delta_{eff,i})$) were converted into the MAFE values for each of the defined damage states. After calculating the MAFE values, estimates of economic losses for each of the identified damage states was obtained by means of the fragility and consequence functions. At the end, MAFE values vs. repair costs were plotted obtaining what is called the loss curve. Integrating the losses over the MAFE domain, the expected annual loss (EAL) was eventually obtained.

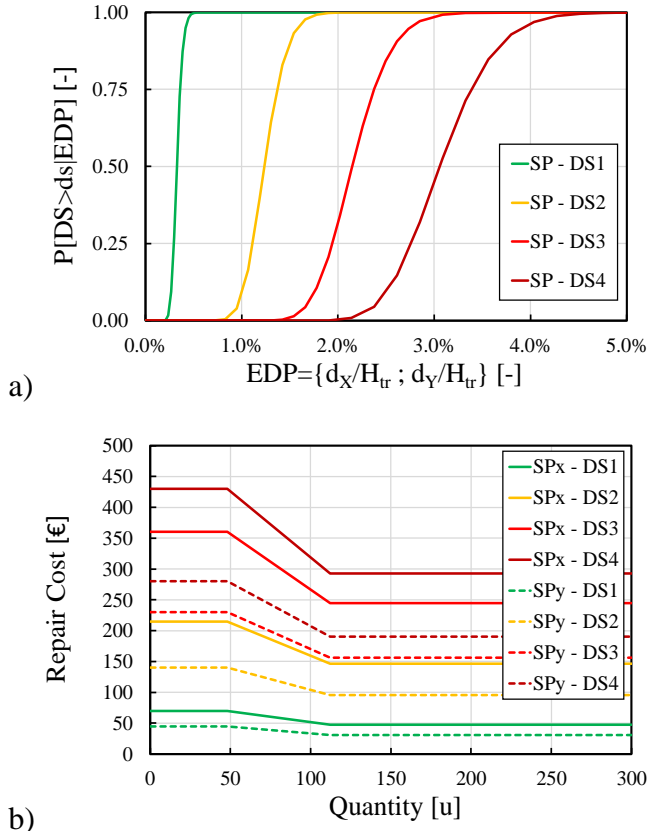


Figure 7. Examples of component fragilities modelling: (a) SP fragility functions; (b) SP repair costs.

6 ANALYSIS RESULTS

6.1 Pushover results

Figure 9(a) summarizes results from pushover analysis in the transverse (X-) direction. As one

can see, both the simplified and full 3D models provide similar results in terms of initial lateral stiffness. The peak shear resistance also was in good agreement among the models. The maximum base shear ratio from the simplified and full 3D models were equal to 0.97 and 0.93, respectively for the cladding made by SPs and TSs. Significant differences are observed in transitions from the elastic to the fully plastic response, especially in the TS case. Besides, significant differences are also noted in the post-peak response. Indeed, the 2D frame model predicts simultaneous failure of truss-to-column connections at all the transverse trusses, because of the rigid diaphragm assumption.

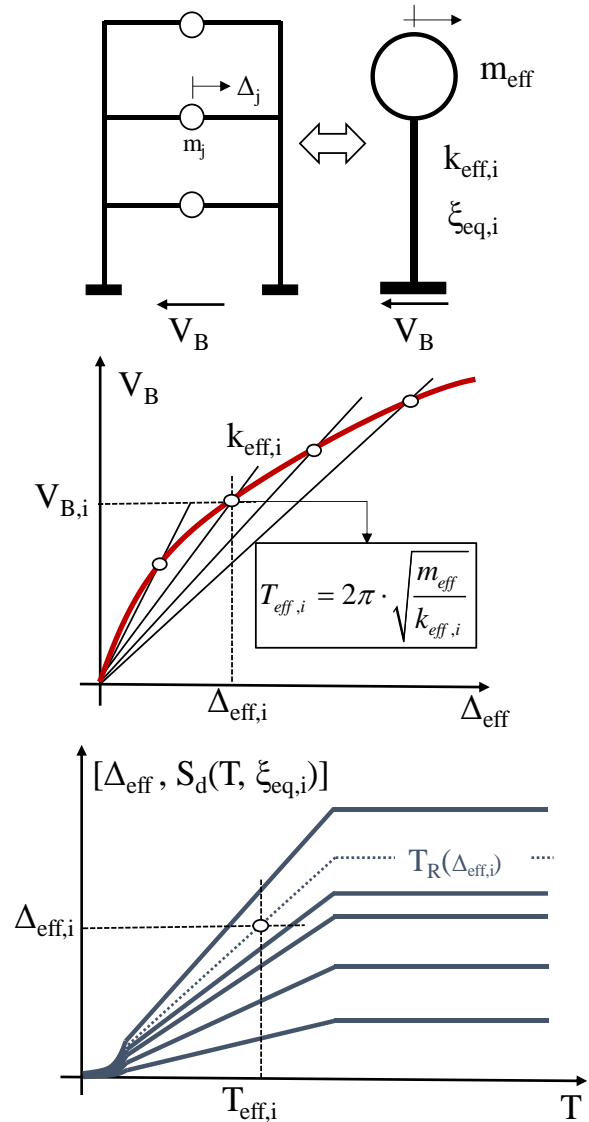


Figure 8. DBLA methodology: graphical description.

Instead, a more continuous behavior is observed for the 3D models with the following relevant aspects: (i) for the building with SPs, after failure of truss-to-column connections, failure of column-to-siderail connections affected the response and limited the cladding

contribution; (ii) for the building with TSs, the roof panels plastic deformations led to a redistribution of internal forces affecting the sequence of truss-to-column connection failure, and leading to different post-peak strength-degrading pushover branch. This consideration holds true also in the case of the building with SPs. Figure 9(b) shows results for the longitudinal (Y-) direction. As for the X-direction, there was agreement between the simplified and full 3D models in terms of both initial lateral stiffness and fully-plastic response branch (i.e., the sub-horizontal branch in the pushover curve).

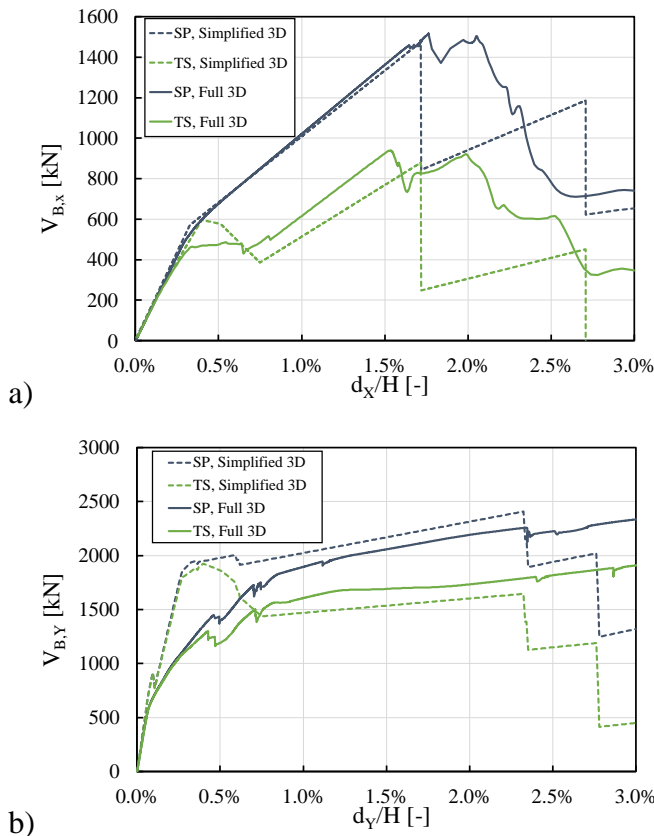


Figure 9. Simplified vs. full 3D models: analysis results; (a) transverse direction; (b) longitudinal direction.

Differences in results were a consequence of the following differences in the models. (i) The absence of modelling the non-linear anchor base connections response in the simplified 3D model. Indeed, the response of the 3D model started to be affected by the inelastic response of column base connections from a lateral drift equal to approximately 0.1%. (ii) Differences in modelling of the brace, and the interaction of two individual brace members at the point of their intersection in the X-configurations. Indeed, the 2D frame model neglected completely such interaction, while in the full 3D model the interaction developed through the explicit

representation of the gusset plate responses. Besides, there were differences in the residual resistance provided by the buckled braces. For the simplified 3D model, the brace residual resistance was obtained from the non-linear modelling guidelines provided by [ASCE SEI 41-13]. For the 3D model, the brace residual resistance was an outcome of the geometrically and materially non-linear model of the brace with equivalent geometric imperfections. As observed in the plot, the ASCE-SEI brace model (implemented in the 2D frame model) predicted the triggering of brace fracture at a lateral drift equal to approximately 2.4%. Brace fracture is not explicitly represented in the 3D model, which consequently shows no loss of resistance even at a drift of 3%.

6.2 Loss curves

Figure 10(a) and Figure 10(b) show comparisons of results for the building X-direction, considering the SP and TS cladding respectively. For the building with SPs, the 3D model predicted economic losses larger than the simplified 3D model at all the MAFE values.

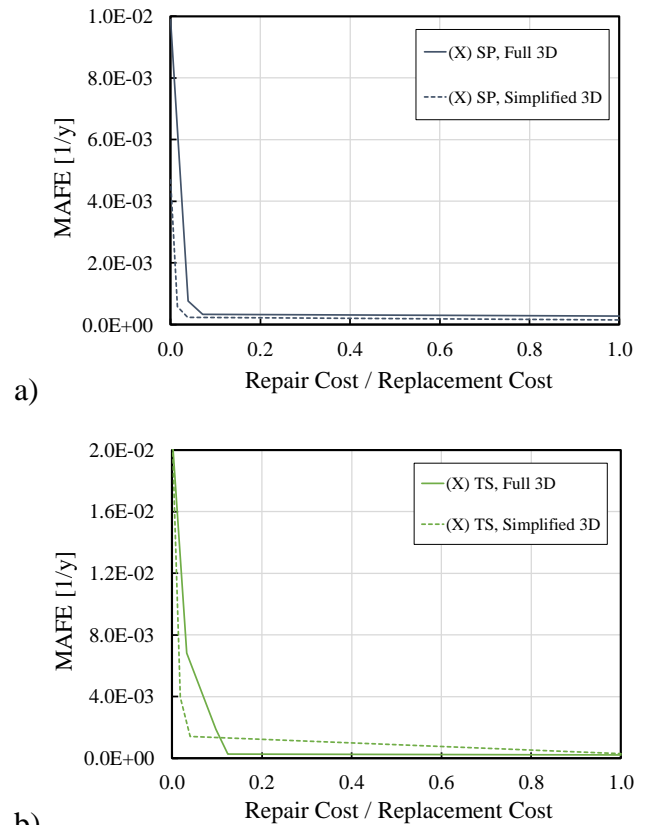


Figure 10. Simplified vs. full 3D models: loss curves for the transverse direction; (a) SP cladding; (b) TS cladding.

This was essentially a consequence of the rigid-diaphragm assumption made for modelling the roof system (roof panels and braces) in the

simplified 3D model. In fact, the rigid diaphragm assumption removed the roof components from the list of damageable components. However, the simplified and full 3D models provided approximately the same values of MAFE to collapse. Consequently, for the building with TS, there is some intersection of the loss curves from the simplified and full 3D models, and at small MAFE values the losses predicted by the simplified 3D model were even larger than the losses obtained using the full 3D model. This overestimation could be reduced by a finer discretization of the pushover response curve from the simplified 3D model. Figure 11(a) and Figure 11(b) summarize the results for the Y-direction. Because of the larger resistance and ductility (compared to the transverse direction, Figure 9), the MAFE to collapse in the longitudinal direction was always smaller than in the transverse direction. Considering that collapse in the transverse direction implies collapse of the whole building, the loss curves for the longitudinal direction were truncated at the minimum MAFE to collapse obtained for the transverse direction. Having used a different scale for the vertical axis, the plots show also in more detail differences in estimation of the MAFE to collapse among the models.

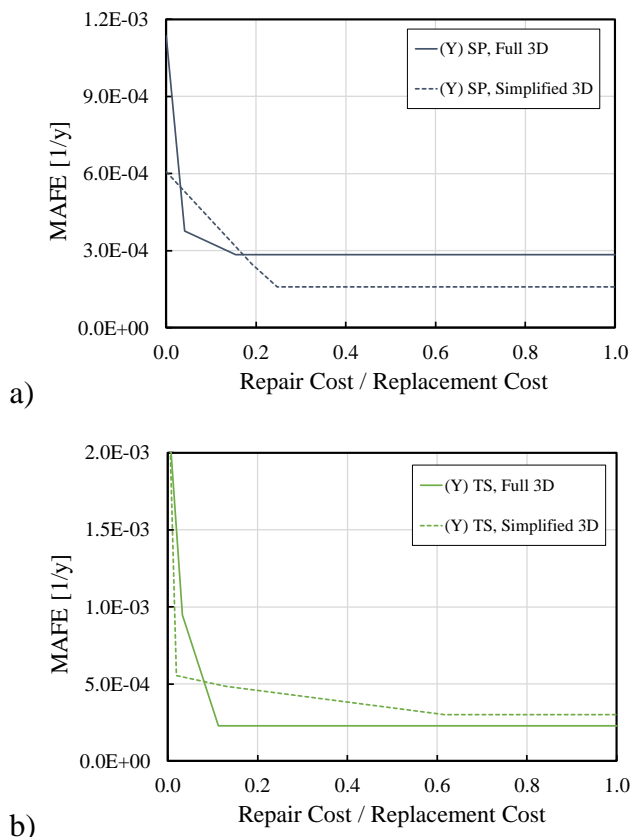


Figure 11. Simplified vs. full 3D models: loss curves for the longitudinal direction; (a) SP cladding; (b) TS cladding.

For both the building with SPs and TS, the zero-loss point (i.e., the anchorage point of the loss curve to the vertical axis) was characterized by smaller MAFE for the simplified 3D models, especially for the SP cladding. This was a consequence of neglecting the contribution of the (ductile) column base connections in the 2D frame models. Therefore, the triggering of damage in the longitudinal direction frames was estimated to occur at a smaller roof displacement and a larger lateral resistance (with correspondingly larger effective stiffness). Hence, the simplified 3D models provided smaller MAFE triggering the initiation of significant damage to the considered building components. Eventually, Figure 12(a) and Figure 12(b) summarize results for the whole building, by summing up the expected losses in the X- and Y-directions, for each MAFE value. Previous observations for the individual directional response hold true also for the whole building.

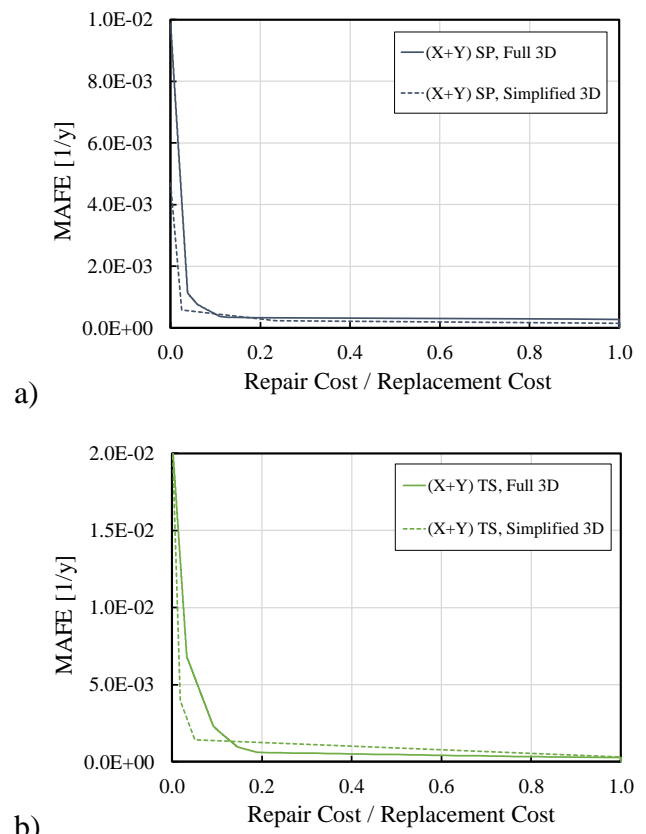


Figure 12. Simplified vs. full 3D models: loss curves for the entire building; (a) SP cladding; (b) TS cladding.

6.3 Expected annual losses (EAL)

The EALs obtained using alternatively the simplified and full 3D models and considering the two cladding types (SP and TS), are provided in Figure 13. The EAL values are reported as

ratios to the building full replacement costs. Comparing results for the different types of cladding, for both the simplified and full 3D models, larger EALs are observed in the case of TS cladding. This result was a consequence of damage to the TS starting prior to global failure of the building. Instead, the building with cladding made of SPs showed smaller EALs, because low cladding damage was observed prior to global failure of the building.

Comparing results for the two building directions, smaller EAL values are observed in the longitudinal direction. The smaller losses were a consequence of the smaller damage observed in the longitudinal components prior to the transverse direction collapse. This result is especially apparent for the TS cladding.

Comparing the simplified and full-3D models, for both cladding types, smaller EAL values are observed for the simplified 3D models. The ratios between the EAL values for the simplified and full 3D models were equal to 0.57 and 0.96, for the SP and TS cladding respectively. This result was a consequence of the rigid diaphragm assumption which was adopted as a simplification for the simplified 3D models. However, underestimation of losses was different varying the cladding type because of the differences in 3D model response. In detail, larger underestimation of EALs are expected in the case of cladding made by SPs, because larger damage was observed in the 3D model roof components. This is a direct consequence of the differences in lateral portal frames stiffness and resistance compared to the internal ones. In the case of cladding made by TSs, as the cladding damage increased, similar stiffness and resistance among the portal frames were observed, leading to a more uniform distribution of roof drifts and, consequently, reducing roof component damage.

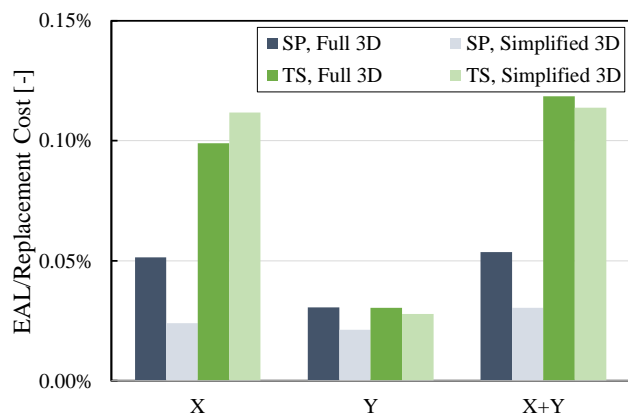


Figure 13. Simplified vs. full 3D model comparison: expected annual losses (EALs).

7 CONCLUSIONS

(i) In the transverse direction and for large MAFE values, significant underestimation of losses resulted from the simplified 3D models, because of the rigid roof assumption. (ii) In the longitudinal direction, significant differences in the evaluation of the zero-loss point were also observed between the simplified and full 3D models, because of neglecting the column base anchor deformations in the simplified models. (iii) The simplified 3D model significantly underestimated the EALs for the SP cladding, due to the rigid roof assumption. On the contrary, rather close EAL values were predicted by the simplified and full 3D models for TS cladding, because the no-loss into roof components were compensated by large damage to the lateral cladding panels. (iv) The simplified and full 3D models predicted rather close values of the MAFE of earthquake intensities causing the building collapse.

REFERENCES

- ASCE, 2014. Seismic evaluation and retrofit of existing buildings, ASCE-SEI 41-13.
- Cantisani G., Della Corte G., 2018. Seismic response of non-conforming single-storey non-residential buildings considering envelope panels, *Proceedings of the Ninth International Conference on Advances in Steel Structures*, Hong Kong, China.
- CEN EN 1993-1-1, 2005. Eurocode 3: Design of steel structure – part 1-1: General rules and rules for buildings, European Committee for Standardization.
- CNR-UNI 10011, 1988. Costruzioni di acciaio: istruzioni per il calcolo, l'esecuzione, il collaudo e la manutenzione.
- CS.LL.PP., 1982. Istruzioni relative ai carichi, ai sovraccarichi ed ai criteri generali per la verifica di sicurezza delle costruzioni (C 24 maggio), *Gazzetta Ufficiale della Repubblica Italiana* 140.
- CS.LL.PP., 1986. Norme tecniche per le costruzioni in zone sismiche (DM 24 Gennaio), *Gazzetta Ufficiale della Repubblica Italiana* 108.
- FEMA P-58, 2012. Seismic performance assessment of buildings, Methodology and Implementation, FEMA.
- McKenna, F., Scott, M.H., Fenves, G.L., 2010. Nonlinear Finite-Element Analysis Software Architecture Using Object Composition, *Journal of Computing in Civil Engineering*, **24**(1): 95–107.
- Porter, K.A., 2003. An Overview of PEER's Performance-Based Earthquake Engineering Methodology, *Proceedings of Ninth International Conference on Applications of Probability and Statistics in Engineering*, San Francisco, CA.
- Welch, D.P., Sullivan, T.J., Calvi, G.M., 2014. Developing direct displacement-based procedures for simplified loss assessment in performance-based earthquake engineering, *Journal of Earthquake Engineering*, **18**(2): 290-322.